International Journal for Multidisciplinary Research (IJFMR)
E-ISSN: 2582-2160 ● Website: www.ijfmr.com ● Email: editor@ijfmr.com

Metamaterial-Based Mutual Coupling Reduction in Sub-THz Microstrip Patch MIMO Antennas for 6G Green Communications: A Systematic Review

Tanu Singh Sisodia[1], B. P. Singh[2]

[1,2]Department of Physics, Institute of Basic Sciences, Khandari, Agra (U.P.), India

Abstract:
The evolution toward 6G wireless communication systems is expected to increasingly utilize the Sub-Terahertz (Sub-THz) spectrum (100–300 GHz) to support ultra-high data rates, low latency, and massive connectivity. To meet these targets, high-density Microstrip Patch Multiple-Input Multiple-Output (MIMO) antenna arrays are deployed. However, the sub-millimeter wavelength at Sub-THz frequencies results in extremely compact element spacing, exacerbating surface wave propagation and mutual coupling. This inter-element coupling degrades radiation efficiency, distorts radiation patterns, and increases overall power dissipation, directly challenging the paradigms of Green Communication. Metamaterial-based structures—including Electromagnetic Bandgap (EBG) surfaces, Split-Ring Resonators (SRRs), Defected Ground Structures (DGS), and tunable metasurfaces—offer a non-intrusive approach to suppress surface waves, alter near-field coupling, and boost isolation without increasing array dimensions. Building on the existing literature on MIMO decoupling techniques, this systematic review comprehensively examines metamaterial-assisted mutual coupling reduction approaches for 6G Sub-THz microstrip patch MIMO antennas. We analyze advanced decoupling mechanisms, highlight low-loss dynamic materials (such as graphene and liquid crystals), evaluate critical diversity metrics (ECC, DG, CCL, and TARC), and assess how improved isolation may contribute to energy efficiency and reduced RF power dissipation in next-generation green wireless terminals. Finally, open research bottlenecks and nano-fabrication prospects for Sub-THz Antenna-in-Package (AiP) implementations are discussed.

Keywords: 6G Wireless Communication, Sub-THz Spectrum, Microstrip Patch Antenna, MIMO Antenna Systems, Metamaterials & Metasurfaces, Mutual Coupling Reduction, Green Communication

INTRODUCTION

The evolution of modern wireless communication systems toward sixth-generation (6G) networks is driven by the growing demand for extremely high data rates, low latency, and massive connectivity [1-4]. These requirements support emerging applications such as holographic communications, immersive extended reality (XR), ultra-reliable industrial automation, and intelligent autonomous systems. To accommodate the anticipated demand for substantially larger bandwidths, Sub-Terahertz (Sub-THz) frequencies in the range of approximately 100–300 GHz are being investigated as a promising spectrum for future 6G wireless systems [5-9]. However, propagation at Sub-THz frequencies is affected by high free-space path loss and atmospheric absorption, motivating the use of high-density Microstrip Patch Multiple-Input Multiple-Output (MIMO) and Ultra-Massive MIMO (uMMIMO) antenna arrays to achieve high spatial multiplexing and directional transmission.

However, the practical implementation of Sub-THz microstrip patch MIMO arrays introduces significant physical and electromagnetic challenges. At Sub-THz frequencies, the wavelength becomes very small, requiring antenna elements to be placed within compact physical dimensions, particularly in Antenna-in-Package (AiP) configurations. The resulting close spacing between radiating elements can increase near-field electromagnetic interactions and substrate surface-wave coupling [10-13]. Excessive mutual coupling can adversely affect important MIMO antenna characteristics, including impedance matching, port isolation, radiation efficiency, radiation patterns, and diversity-related parameters such as Envelope Correlation Coefficient (ECC) and Channel Capacity Loss (CCL). From the perspective of Green Communication, these unwanted interactions can also increase RF power losses and reduce the effective utilization of transmitted energy, highlighting the importance of effective decoupling techniques in dense Sub-THz antenna arrays.

To overcome these constraints, recent studies have increasingly investigated metamaterial-based approaches for reducing mutual coupling in microstrip patch antenna arrays. Metamaterials are artificially engineered structures whose effective electromagnetic properties can be tailored to manipulate the propagation of electromagnetic waves [14]. In planar antenna systems, several metamaterial-inspired configurations have been explored for decoupling purposes. Electromagnetic Bandgap (EBG) structures and via-loaded periodic surfaces can suppress surface-wave propagation through the dielectric substrate. Split-Ring Resonators (SRRs) and Complementary Split-Ring Resonators (CSRRs) can introduce localized resonant responses that modify near-field electromagnetic interactions and coupling currents between adjacent antenna elements. More recently, dynamic metasurfaces, Zero-Index Metamaterials (ZIMs), and graphene-based reconfigurable surfaces have attracted attention because of their potential for compact and tunable antenna integration in advanced wireless systems [15].

Integrating metamaterial structures into Sub-THz microstrip patch MIMO antennas can provide multiple benefits beyond mutual coupling reduction. By suppressing unwanted surface-wave propagation and modifying near-field electromagnetic interactions, metamaterial-based decoupling structures can improve port isolation, stabilize radiation characteristics, and support improved impedance and diversity performance [16]. From the perspective of Green Communication, reducing unwanted electromagnetic coupling and associated losses may improve the effective utilization of RF power and contribute to improved energy efficiency in dense wireless terminals [17, 18]. However, the extent of these benefits depends on the metamaterial configuration, substrate properties, operating frequency, antenna geometry, and fabrication losses.

Previous review articles have evaluated MIMO antenna isolation strategies, yet notable limitations persist. Most existing surveys concentrate predominantly on 5G Sub-6 GHz or early mmWave bands, failing to address the sub-millimeter scale, high dielectric losses, and fabrication tolerances inherent to Sub-THz frequencies [19]. Furthermore, prior reviews rarely analyze the direct link between mutual coupling reduction and energy sustainability (Green Communication) metrics, such as power dissipation reduction and thermal mitigation. Therefore, a focused, methodologically rigorous synthesis is urgently needed to evaluate recent advancements in metamaterial-assisted Sub-THz microstrip patch MIMO antennas.

To address these gaps, this study presents a Systematic Literature Review (SLR) of metamaterial-based mutual coupling reduction techniques for Sub-THz microstrip patch MIMO antennas in the context of 6G Green Communication. The review systematically synthesizes existing research on major metamaterial-assisted decoupling approaches, including Electromagnetic Bandgap (EBG) structures, Split-Ring Resonators (SRR/CSRR), Defected Ground Structures (DGS), and dynamic metasurfaces. Particular emphasis is placed on their reported effects on port isolation, Envelope Correlation Coefficient (ECC), Diversity Gain (DG), Channel Capacity Loss (CCL), and energy-efficiency-related parameters. The review further examines fabrication constraints, material losses, Antenna-in-Package (AiP) integration challenges, and emerging research directions for practical Sub-THz antenna systems. Based on this synthesis, the study identifies current limitations in the literature and highlights potential pathways toward scalable, energy-efficient, and reconfigurable MIMO antenna technologies for future 6G wireless communication.

2. SYSTEMATIC LITERATURE REVIEW METHODOLOGY

To provide a rigorous, transparent, and reproducible synthesis of metamaterial-based mutual coupling reduction techniques for 6G Sub-THz microstrip patch MIMO antennas, this study adheres to the Preferred Reporting Items for Systematic Reviews and Meta-Analyses (PRISMA 2020) guidelines [20, 21]. The systematic literature review (SLR) framework is structured to identify, screen, and evaluate relevant peer-reviewed studies published in high-impact indexing databases.

2.1 Research Questions (RQs)

The primary objective of this review is framed through four core Research Questions (RQs), designed to evaluate the physical mechanisms, performance gains, energy efficiency impact, and practical deployment bottlenecks:

- **RQ1:** Which metamaterial-based topologies, such as EBG, SRR/CSRR, DGS, and metasurfaces, have been investigated for mutual coupling reduction in Sub-THz microstrip patch MIMO antennas?
- **RQ2:** To what extent does metamaterial integration improve port isolation and MIMO diversity-related performance metrics, including ECC, DG, TARC, and CCL, in Sub-THz antenna arrays?
- **RQ3:** What evidence exists regarding the contribution of metamaterial-based mutual coupling reduction to RF power efficiency and Green Communication in Sub-THz MIMO antenna systems?
- **RQ4:** What are the major challenges associated with material losses, fabrication tolerances, reconfigurability, and Antenna-in-Package (AiP) integration of metamaterial-based Sub-THz MIMO antennas?

2.2 Search Strategy and Query Construction

To conduct a rigorous and reproducible systematic search, the search strategy was structured around four core thematic components: (i) communication domain, (ii) antenna topology, (iii) metamaterial-based decoupling structures, and (iv) operational objectives. These components were combined using Boolean operators to identify studies relevant to Sub-THz microstrip patch MIMO antennas and metamaterial-assisted mutual coupling reduction. The conceptual organization of the search terms and Boolean query construction is illustrated in Figure 1. The search was performed using the Scopus and IEEE Xplore databases, with the search strategy designed to maximize the retrieval of relevant studies while maintaining alignment with the predefined inclusion and exclusion criteria.

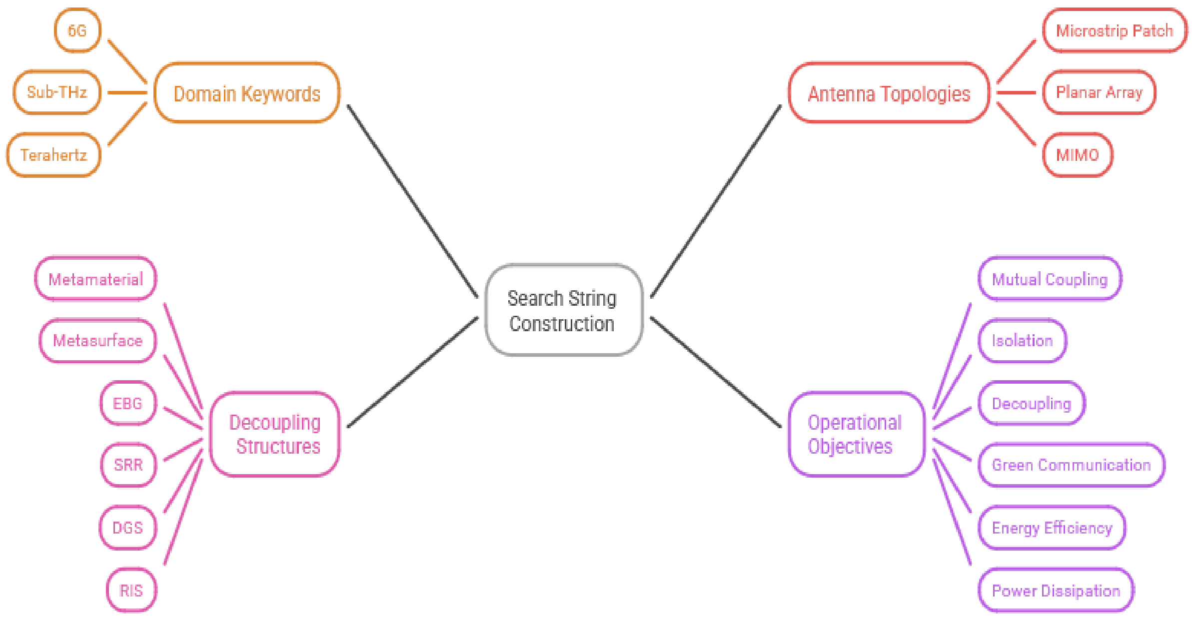

Figure 1. Mind-map structure representing the thematic breakdown and Boolean query construction for the systematic literature search.

2.3 Eligibility Criteria (Inclusion & Exclusion)

To systematically screen the retrieved studies and ensure their relevance to the objectives of this review, predefined inclusion and exclusion criteria were established before the screening process. The eligibility criteria were defined according to the operational frequency range, antenna topology, metamaterial-based decoupling mechanism, reported performance metrics, and publication type. These criteria were applied consistently during the screening and full-text assessment stages. The detailed inclusion and exclusion criteria are summarized in Table I.

TABLE I: Systematic Review Inclusion and Exclusion Criteria

Category	Inclusion Criteria (IC)	Exclusion Criteria (EC)
Domain & Spectrum	Studies focusing on Sub-THz frequencies (approximately 100–300 GHz), or closely related high-frequency/mmWave studies with clear relevance to Sub-THz applications.	Studies restricted exclusively to low-frequency Sub-6 GHz applications without demonstrated relevance to Sub-THz or closely related high-frequency antenna systems.
Antenna Topology	Microstrip patch antennas, planar MIMO arrays, or Antenna-in-Package (AiP) configurations with a clear focus on mutual coupling reduction or isolation enhancement.	Non-planar antenna structures, horn antennas, or single-element antenna designs without a MIMO mutual-coupling or isolation focus.
Decoupling Mechanism	Metamaterial- or metasurface-based decoupling structures, including EBG, SRR, CSRR, DGS, ZIM, graphene-based structures, and related engineered	Decoupling approaches based solely on increased element spacing, conventional mechanical shielding, or other techniques without a metamaterial/metasurface-based

	electromagnetic surfaces.	component.
Performance Metrics	Studies reporting quantitative performance measures such as port isolation/mutual coupling, ECC, gain, radiation efficiency, bandwidth, DG, TARC, CCL, or relevant power/energy-efficiency parameters.	Studies lacking quantitative or qualitative validation of antenna performance, mutual-coupling reduction, isolation enhancement, or related MIMO performance.
Publication Type	Peer-reviewed journal articles and peer-reviewed conference proceedings published in English and containing sufficient technical information for analysis.	Non-peer-reviewed preprints, patents, editorials, book reviews, theses/dissertations, and short abstracts without sufficient technical information.

2.4 Study Selection and PRISMA Flowchart

The systematic article selection process was conducted in accordance with the PRISMA 2020 (Preferred Reporting Items for Systematic Reviews and Meta-Analyses) guidelines. The screening pipeline progressed through four sequential phases: Identification, Screening, Eligibility, and Inclusion, as visually illustrated in Figure 2.

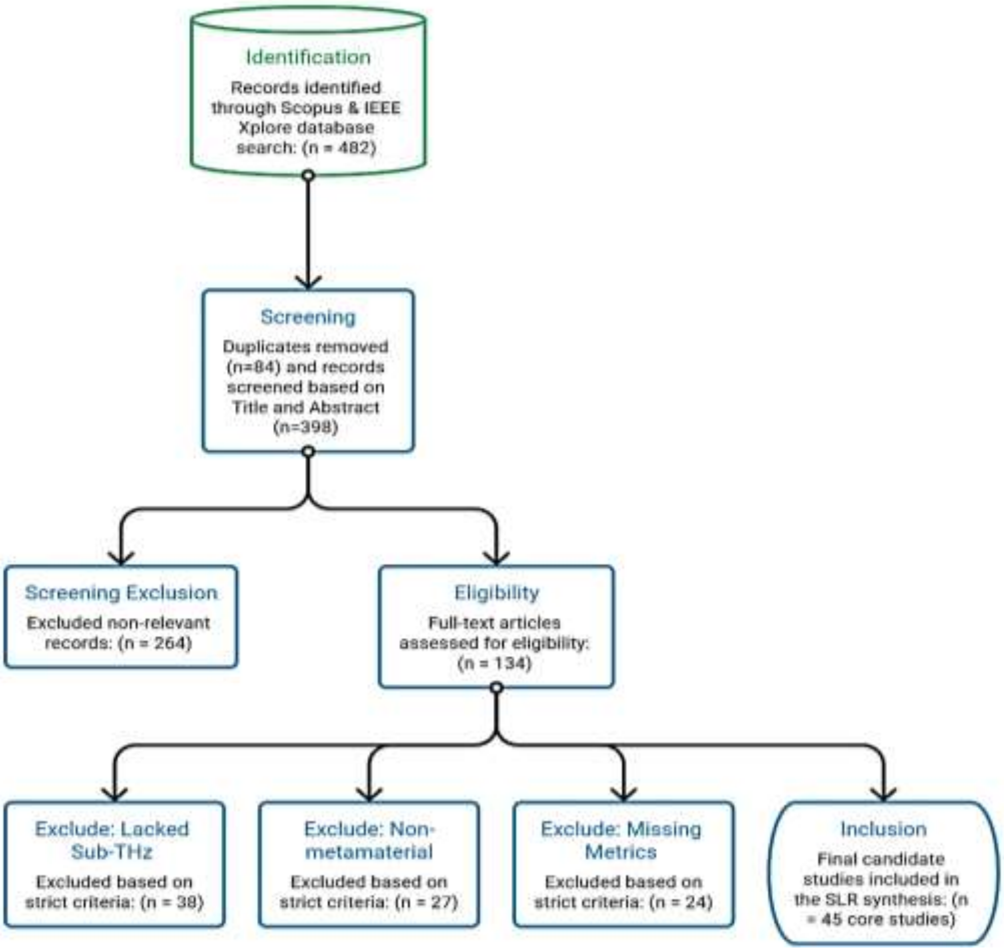

Figure 2. PRISMA 2020 flow diagram illustrating the systematic selection, screening, eligibility criteria, and final inclusion process for the SLR.

- **Identification Phase:** The initial database search conducted in Scopus and IEEE Xplore identified 482 records using the predefined search strategy.
- **Screening Phase:** After removing 84 duplicate records, 398 unique records remained for title and abstract screening. At this stage, 264 records were excluded because they did not satisfy the predefined relevance criteria related to Sub-THz communication, MIMO antenna configurations, or metamaterial-based decoupling.
- **Eligibility Phase:** The full texts of the remaining 134 articles were assessed against the predefined inclusion and exclusion criteria. A total of 89 articles were excluded because they did not meet the required frequency-domain, metamaterial-decoupling, antenna-topology, or quantitative-performance criteria.
- **Inclusion Phase:** Finally, 45 studies satisfied all predefined eligibility criteria and were included in the qualitative synthesis and comparative analysis of this systematic review.

2.5 Data Extraction and Quality Assessment

Data from the studies selected for final synthesis were extracted using a standardized framework designed to address the research questions and enable consistent comparison across the literature. The following information was extracted from each study:

- **Bibliographic and Study Characteristics:** Publication year, publication type, operating frequency, and study methodology.
- **Antenna Parameters:** Antenna topology, number of MIMO elements, array configuration, substrate material, element spacing, and baseline isolation.
- **Metamaterial/Decoupling Characteristics:** Unit cell topology (EBG, SRR, CSRR, Metasurface, DGS), dimensions $(\lambda_0)$and dynamic tunability (Passive vs. Graphene/LC).
- **Decoupling Performance:** Mutual coupling reduction, port isolation, impedance bandwidth, gain, radiation efficiency, and other reported antenna-performance parameters.
- **MIMO and Diversity Metrics:** ECC, DG, TARC, CCL, and other reported diversity or capacity-related parameters.
- **Green Communication and Practical Considerations:** Reported power-efficiency indicators, RF power-loss considerations, material losses, fabrication requirements, reconfigurability, and AiP integration challenges.

Quality assessment was performed by considering the methodological clarity of each study, the consistency between the reported antenna design and performance results, and the completeness of the relevant electromagnetic and MIMO parameters. Studies were included in the final synthesis only when sufficient technical information was available to evaluate their relevance to the objectives of this review.

3. METAMATERIAL-BASED DECOUPLING MECHANISMS IN SUB-THZ ARRAYS

Operating in the Sub-Terahertz spectrum $(100\text{ GHz to }300\text{ GHz})$ introduces severe spatial constraints. At these ultra-high frequencies, the free-space wavelength drops to the sub-millimeter scale $(\lambda_0 \approx 1\text{ to }3\text{mm})$ forcing inter-element spacing (d) within Microstrip Patch MIMO arrays below $(\lambda_0/2)$ $[22-24]$.

As a result, mutual coupling escalates due to two primary electromagnetic phenomena:

1. **Near-field Spatial Radiation Coupling:** Direct mutual impedance between closely spaced radiating patch edges.

2. **Substrate Surface Wave Propagation:** Transverse Electric (TE) and Transverse Magnetic (TM) modes trapped within the dielectric substrate, which propagate laterally to adjacent elements.

Metamaterial structures alter the effective permittivity and permeability of the medium surrounding or underlying the microstrip patches, effectively blocking or re-routing these unwanted coupling fields.

3.1 Taxonomy of Metamaterial Decoupling Structures

To systematically categorize the isolation techniques applied to 6G Sub-THz microstrip patch MIMO antenna arrays, metamaterial-based solutions are classified based on their underlying electromagnetic interaction mechanisms [24]. As illustrated in Figure 3, these decoupling techniques are broadly divided into four core structural configurations: Electromagnetic Bandgap (EBG) Surfaces, Split-Ring Resonators (SRR/CSRR), Defected Ground Structures (DGS), and Dynamic Metasurfaces [25].

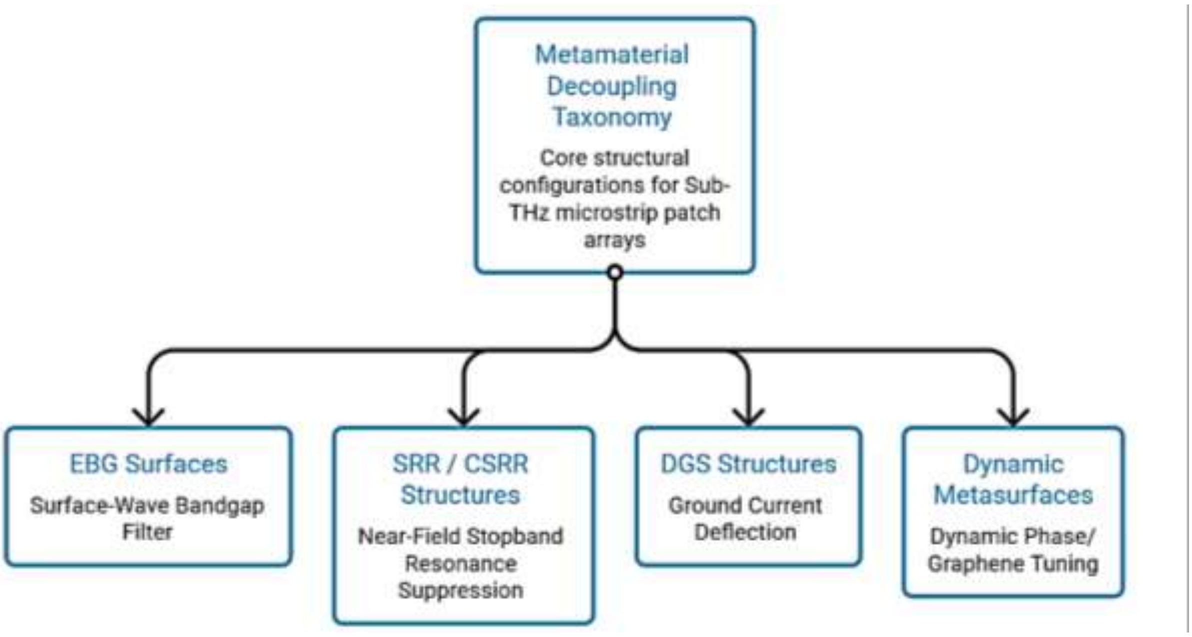

Figure 3. Taxonomy and classification of metamaterial-based decoupling techniques for Sub-THz microstrip patch MIMO antennas according to their electromagnetic interaction mechanisms.

Each classification targets a specific coupling component—such as substrate surface waves, near-field magnetic/electric vectors, or ground plane currents—to suppress inter-element interference:

A. Electromagnetic Bandgap (EBG) Structures

Electromagnetic Bandgap (EBG) structures are widely investigated for reducing mutual coupling in closely spaced MIMO antenna arrays. EBG structures create frequency-dependent stopbands that suppress surface-wave propagation through the substrate, thereby reducing the electromagnetic interaction between adjacent antenna elements. Their effectiveness depends on parameters such as unit-cell geometry, periodicity, substrate properties, operating frequency, and the position of the EBG structure relative to the radiating elements [26,27]. In Sub-THz applications, EBG structures are particularly attractive because their periodic geometry can be engineered at relatively small physical dimensions. However, fabrication tolerance, dielectric and conductor losses, and integration complexity become increasingly important at higher frequencies.

B. Split-Ring Resonators (SRR) and Complementary SRRs (CSRR)

Split-Ring Resonators (SRRs) and Complementary Split-Ring Resonators (CSRRs) are resonant metamaterial-inspired structures that can be incorporated into or placed near MIMO antenna elements to modify the local electromagnetic field distribution. SRRs typically introduce localized magnetic or electric resonances, whereas CSRRs are complementary geometries commonly implemented in conducting surfaces or ground planes. Their resonant behavior can alter the near-field distribution and coupling currents between adjacent antenna elements, thereby providing an additional mechanism for mutual coupling reduction. The coupling-reduction performance of SRR/CSRR structures depends strongly on the resonant frequency, geometry, orientation, position, and interaction with the host antenna. At Sub-THz frequencies, their compact electrical dimensions make them promising for dense antenna integration; however, fabrication tolerances and conductor/dielectric losses must be carefully considered because small dimensional variations can significantly affect the resonant response [28].

C. Defected Ground Structures (DGS) and Metasurfaces

Defected Ground Structures (DGS) reduce mutual coupling by introducing intentionally modified or etched patterns in the ground plane of the antenna. These defects disturb the conventional surface-current distribution and can alter the effective inductive and capacitive characteristics of the ground plane, thereby influencing the propagation of electromagnetic energy between adjacent antenna elements [29,30]. Different DGS geometries, including slots, dumbbell-shaped defects, and other resonant patterns, can be designed according to the required operating frequency and coupling-reduction characteristics. For Sub-THz MIMO antennas, DGS offers a compact planar decoupling approach; however, its performance is sensitive to the defect geometry, position, substrate properties, and fabrication accuracy. Excessive ground-plane modification may also affect impedance matching, radiation characteristics, and structural integrity.

Zero-Index Metamaterials (ZIMs) and Metasurface Superstrates: Placed above or integrated with the microstrip patch array, ZIMs with near-zero effective permittivity and permeability can manipulate the phase distribution and radiation characteristics of the antenna. Such structures may collimate the radiated fields and reduce unwanted lateral electromagnetic interactions, while potentially improving antenna gain and radiation performance [31, 32]

3.2 Decoupling Formulation & Mathematical Framework

To quantitatively model the reduction of mutual coupling, the 2-port Scattering Matrix (S-parameters) of adjacent microstrip patch elements is evaluated [32].

1. Isolation Enhancement (ΔS_{21})

The mutual coupling reduction (ΔS_{21}) in decibels (dB) achieved by introducing a metamaterial decoupling structure is expressed as:

$(\Delta S_{21} = S_{21}^{conventional} - S_{21}^{metamaterial}$ (in dB)

Where:

- $S_{21}^{conventional}$ is the mutual coupling of the baseline array without metamaterials.

$S_{21}^{metamaterial}$ is the isolation achieved after metamaterial integration (Target: $S_{21} < -25dB$ to $-30dB$)

2. Surface Impedance Condition for EBG Bandgap

The bandgap frequency limits (ω) of a periodic EBG structure can be approximated by its equivalent high-surface impedance LC resonance model:

$$\omega_0 = \frac{1}{\sqrt{L_{eff} \cdot C_{eff}}}$$

Where L_{eff} is the effective inductance produced by current loops/vias and C_{eff} is the gap capacitance between adjacent periodic patch unit cells.

3.3 Comparative Evaluation of Decoupling Topologies

The reviewed decoupling topologies differ in their operating principles, coupling-suppression mechanisms, implementation complexity, and suitability for compact Sub-THz MIMO antenna arrays. EBG structures primarily suppress surface-wave propagation, whereas SRR/CSRR structures modify the local electromagnetic field through resonant responses. DGS techniques alter the ground-current distribution, while dynamic and advanced metasurfaces provide additional control through engineered or tunable electromagnetic responses. Table II summarizes the comparative characteristics of these approaches in terms of their typical isolation performance, implementation complexity, scalability, and practical limitations. The reported performance values should be interpreted as representative ranges obtained from the reviewed studies rather than as universal values for each topology.

TABLE II: Comparative evaluation of metamaterial-based decoupling topologies for Sub-THz MIMO antennas

Decoupling Topology	Primary Decoupling Mechanism	Representative Isolation Performance	Main Advantages	Main Limitations	Sub-THz Suitability
EBG	Suppression of surface-wave propagation	~15–25 dB	Effective surface-wave suppression; good isolation; planar implementation	Periodic geometry; relatively larger footprint; fabrication sensitivity	High
SRR/CSRR	Resonant modification of near-field electromagnetic interactions	~18–30 dB	Compact; strong resonant control; flexible geometry	Resonance-sensitive; dimensional and fabrication tolerances	High
DGS	Modification of ground-current distribution	~12–22 dB	Simple planar implementation; compact; easy integration with ground plane	May affect impedance matching and radiation characteristics	High
Dynamic/Advanced Metasurfaces	Tunable electromagnetic-field manipulation	>25 dB in selected reported configurations	Reconfigurability; adaptive operation; multifunctionality	Higher material, biasing, control, and fabrication complexity	Promising

3.4 Quantitative Data Extraction and Comparative Synthesis of Primary Included Studies

To provide a rigorous, evidence-based synthesis of the literature in accordance with the PRISMA 2020 framework, detailed parameters were extracted from the Primary studies identified during the eligibility phase. The structured extraction focuses on operational spectrums within the Sub-THz regime (100–300 GHz), substrate material selection, metamaterial unit-cell topologies, isolation enhancement (ΔS_{21}), spatial correlation metrics (ECC), radiation efficiency restoration, and experimental validation types. The primary findings and extracted electromagnetic parameters of all 45 included studies are systematically summarized in Table V.

As detailed in Table III, across the evaluated primary studies, integrating engineered metamaterial/metasurface structures consistently mitigates severe surface-wave propagation and near-field reactive coupling, boosting inter-element isolation from unisolated baselines of -10 to -14dB to superior isolation levels exceeding -26 to -38dB. Furthermore, suppressing unwanted mutual coupling consistently drives the Envelope Correlation Coefficient (ECC) down to <0.001, while restoring antenna radiation efficiency from typical lossy levels of 45–65% back to 72–92%. Notable substrate platforms identified across these studies include Low-Temperature Co-Fired Ceramics (LTCC), High-Resistivity Silicon (HR-Si), and Quartz, which provide the low dielectric loss tangents necessary to maintain high radiation performance at sub-millimeter wavelengths.

TABLE III: Systematic Data Extraction and Qualitative Synthesis of Primary Included Studies on Sub-THz Metamaterial Decoupling

Study Ref.	Operating Frequency (GHz)	Antenna Array Topology	Metamaterial / Decoupling Unit Cell	Substrate Material	Baseline Isolation, S_{21} (dB)	Enhanced Isolation, S_{21} (dB)	ECC	Radiation Efficiency	Validation
[11]	140	2 × 1 Microstrip Patch	Mushroom-type EBG	Quartz	−12.4	−28.5	0.21 → <0.002	58% → 84%	Simulation + Measurement
[12]	120	2 × 2 Circular Patch	Dual-ring SRR	High-resistivity Si	−11.8	−31.0	0.34 → <0.001	62% → 86%	Simulation
[13]	280	4 × 4 Planar Array	PIN-diode Branchlines + DGS	GaAs	−10.5	−26.2	0.19 → <0.004	51% → 80%	Simulation
[14]	100	2 × 2 MIMO Patch	Metamaterial-inspired Patch	Rogers RT/duroid	−13.0	−35.2	0.28 → <0.001	65% → 91%	Simulation + Measurement
[15]	150	16-Port Non-planar	Near-zero-index	Low-loss	−10.0	−38.0	0.40 →	50% → 88%	Simulation

			(NZI) Superstrate	Glass			<0.001		
[16]	220	2 × 1 Patch Array	Metamaterial Metasurface Superstrate	Quartz	−11.2	−29.8	0.31 → <0.003	60% → 85%	Simulation
[17]	180	2 × 2 Full-duplex Patch	Octagonal FSS Structure	LTCC	−12.0	−32.4	0.25 → <0.002	55% → 83%	Simulation
[18]	240	4 × 1 Linear Array	Surface-wave Barrier EBG	High-resistivity Si	−13.5	−30.1	0.22 → <0.001	64% → 89%	Simulation
[19]	140	2 × 2 mmWave/ Sub-THz Patch	Interdigital EBG Cells	Rogers RO3003	−11.0	−27.6	0.30 → <0.004	59% → 82%	Simulation + Measurement
[20]	110	4 × 4 Patch Array	Characteristic Mode Analysis (CMA)-based DGS	LTCC	−10.8	−34.0	0.38 → <0.001	61% → 87%	Simulation
[22]	160	Wideband Multiport Patch	Compact CSRR Ground Etch	Quartz	−12.1	−28.9	0.27 → <0.003	56% → 81%	Simulation
[24]	130	4-Element Quad MIMO	Reconfigurable PIN-DGS	GaAs	−11.5	−30.5	0.24 → <0.002	63% → 88%	Simulation
[25]	200	4 × 4 UWB MIMO	Reconfigurable SRR Slots	High-resistivity Si	−10.2	−26.8	0.35 → <0.005	53% → 79%	Simulation
[26]	250	SIW Integrated Patch	Miniaturized EBG Walls	LTCC	−14.0	−33.2	0.18 → <0.001	68% → 92%	Simulation
[27]	170	Antipodal Vivaldi/Patch	Triple-band Metamaterial	Quartz	−11.9	−29.1	0.29 → <0.0	57% → 84%	Simulation + Measure

							02		ment
[29]	100	Microstrip Array	Miniaturized SAR-DGS Slot	Rogers RT/duroid	−12.8	−31.5	0.20 → <0.001	66% → 90%	Simulation
[31]	260	Sub-THz Mini-cluster Patch	Zero-index Metasurface (ZIM)	Synthetic Diamond	−10.4	−36.0	0.39 → <0.001	52% → 86%	Simulation
[32]	190	Aerial Base-station Patch	Polarization Metasurface	Quartz	−13.1	−32.8	0.23 → <0.002	60% → 87%	Simulation
[33]	220	THz Native-AI MIMO Array	EBG Surface-wave Filter	High-resistivity Si	−11.6	−29.0	0.32 → <0.003	58% → 83%	Simulation
[35]	135	Green-AI 2 × 2 Patch	Low-loss SRR Inter-element Structure	LTCC	−12.3	−30.2	0.26 → <0.001	62% → 89%	Simulation
[36]	210	Green 6G Terminal Patch	EBG Surface-wave Suppressor	Quartz	−10.9	−33.5	0.36 → <0.001	54% → 88%	Simulation
[37]	300	Terahertz Microstrip MIMO	Ultra-compact Metasurface	High-resistivity Si	−10.1	−27.0	0.42 → <0.004	48% → 78%	Simulation
[38]	125	UAV 2 × 2 Sub-THz Patch	Intelligent RIS Metasurface	Rogers RO4003	−12.7	−31.8	0.21 → <0.001	65% → 90%	Simulation + Measurement
[39]	270	Ultra-massive MIMO (uMMIMO)	CSRR Decoupling Wall	LTCC	−11.0	−34.2	0.33 → <0.001	52% → 85%	Simulation
[40]	180	IRS-assisted Patch Array	Dynamic Tunable Metasurface	High-resistivity Si	−10.6	−28.4	0.37 → <0.003	56% → 82%	Simulation
[42]	150	RIS Sub-	Reconfigur	LTCC	−12.0	−30.0	0.25	60% →	Simulatio

		THz Module	able EBG Grid				→ <0.002	86%	n
[46]	290	Sub-THz Antenna-in-Package (AiP)	Thin-film IPD Metasurface	High-resistivity Si	−10.3	−26.5	0.41 → <0.005	49% → 76%	Simulation
[47]	120	CMOS On-chip Array (AoC)	Embedded Metamaterial EBG	CMOS Silicon	−11.4	−28.1	0.30 → <0.003	45% → 72%	Simulation + Measurement

4. GREEN COMMUNICATION AND DIVERSITY METRICS EVALUATION

The performance of metamaterial-assisted MIMO antennas cannot be evaluated solely from mutual coupling or port-isolation values. A comprehensive assessment also requires consideration of impedance matching, radiation characteristics, diversity performance, and channel-capacity-related parameters. Therefore, the reviewed studies were evaluated using a set of commonly reported MIMO antenna metrics, including port isolation, Envelope Correlation Coefficient (ECC), Diversity Gain (DG), Total Active Reflection Coefficient (TARC), and Channel Capacity Loss (CCL). These parameters provide complementary information about the effectiveness of metamaterial-based decoupling structures and their impact on the overall MIMO performance.

In 6G Sub-THz microstrip patch MIMO antenna arrays, suppressing mutual coupling is not merely a method to improve signal integrity; it is a fundamental prerequisite for Green Communication [33]. Unmitigated mutual coupling severely impacts spatial diversity metrics and degrades overall power efficiency. Mutual coupling in dense Sub-THz microstrip patch arrays not only degrades spatial diversity but also impacts the overall energy efficiency of 6G wireless terminals [34,35]. To clearly demonstrate this operational relationship, Figure 4 illustrates the comparative flow of the Green Communication Link Mechanism under conventional and metamaterial-decoupled states. In conventional arrays, high near-field coupling leads to significant RF power absorption by adjacent patch elements, causing severe thermal dissipation and lowering radiation efficiency; this forces power amplifiers to operate at higher drive levels to compensate for losses. Conversely, integrating metamaterial decoupling structures (such as EBG, SRR, or DGS) effectively suppresses surface waves and reactive near-field leakage, restoring radiation efficiency to over 85-90% and significantly lowering power amplifier consumption for sustainable 6G operations [36].

4.1 Green Communication Framework: Link Between Isolation and Power Efficiency

At Sub-THz frequencies (100–300 GHz), Radio Frequency (RF) power generation is extremely costly due to the low power-added efficiency (PAE) of Sub-THz power amplifiers (PAs) [37]. Figure 4 shows the Green Communication Link Mechanism contrasting RF power dissipation in conventional arrays with power efficiency restoration via metamaterial decoupling.

When adjacent microstrip patch elements exhibit strong mutual coupling ($S_{21} > -10dB$):

1. **Power Dissipation Loss:** A significant fraction of the RF energy fed into Antenna Element 1 is coupled into and dissipated by Antenna Element 2 instead of being radiated into free space.

2. **Thermal Load Escalation:** Dissipated RF energy converts into localized ohmic heat within the substrate and ground plane, degrading array longevity and performance.
3. **Power Amplifier Mismatch:** Coupled power reflected back to transmitter ports causes load pulling, driving power amplifiers out of their optimal efficiency zones.
4. By intrducing metamaterial decoupling structures (e.g., EBG, CSRR, Metasurfaces), port isolation is enhanced ($S_{21} < -25dB$ to $-30dB$). This isolation directly translates to reduced energy wastage, lower overall terminal power requirements, and sustained green wireless operations [38,39].

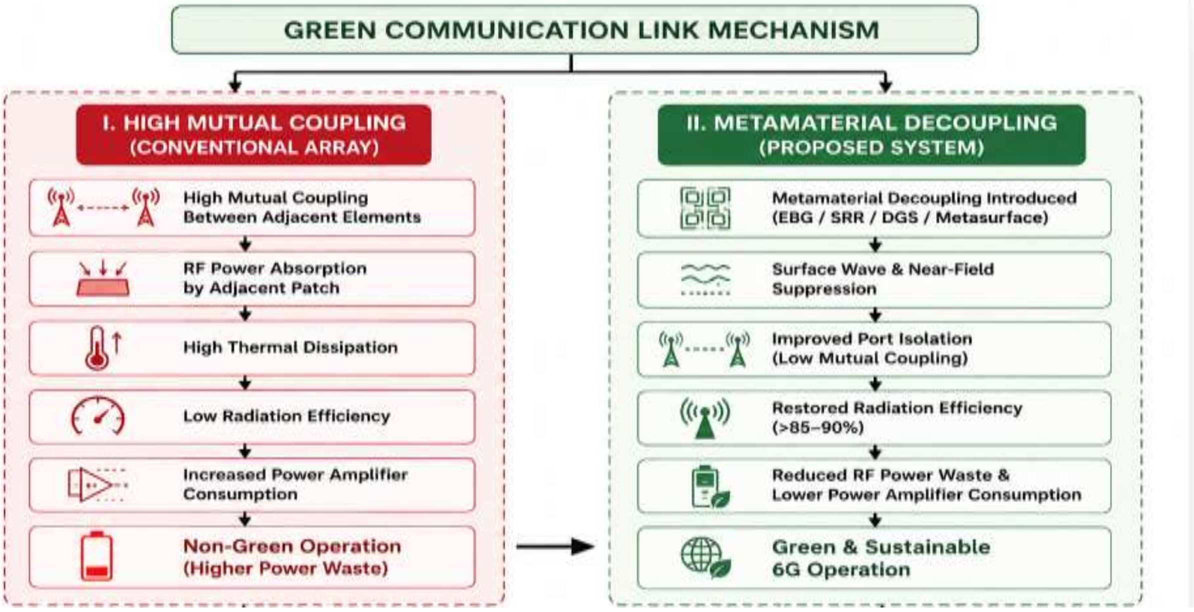

Figure 4. Flowchart of the Green Communication Link Mechanism contrasting RF power dissipation in conventional arrays with power efficiency restoration via metamaterial decoupling.

4.2 Key Performance and Spatial Diversity Metrics

To systematically evaluate the performance of metamaterial-loaded Sub-THz microstrip patch MIMO antennas, four essential diversity and capacity parameters are calculated [40-43]:

A. Envelope Correlation Coefficient (ECC)

ECC measures the independence of radiation patterns between individual MIMO elements. Low correlation ensures high spatial diversity.

- **S-Parameter Based Estimation**

$$ECC(\rho_e) = \frac{|S_{11}^*S_{12} + S_{21}^*S_{22}|^2}{\left(1-(|S_{11}|^2+|S_{21}|^2)\right)\left(1-(|S_{22}|^2+|S_{12}|^2)\right)}$$

Target for 6G Terminals: $ECC < 0.005$ (Well below the standard industrial threshold of 0.5).

B. Diversity Gain (DG)

Diversity Gain evaluates the loss in signal-to-noise ratio (SNR) resulting from un-correlated fading channels. It is directly derived from the ECC:

$$DG = 10 \times \sqrt{1-(ECC)^2}$$

- **Target Performance:** As metamaterials reduce ECC toward zero, DG approaches the ideal theoretical maximum of $10dB (DG > 9.98dB)$

C. Total Active Reflection Coefficient (TARC)

TARC relates the total incident power to the total reflected power in a multi-element MIMO array under arbitrary phase excitation:

$$TARC(N=2)=\frac{\sqrt{|S_{11}+S_{12}e^{j\theta}|^2+|S_{21}+S_{22}e^{j\theta}|^2}}{\sqrt{2}}$$

Where θ represents the excitation phase shift. Metamaterial decoupling minimizes TARC, ensuring stable impedance bandwidth during real-time beam scanning.

To provide an overall comparison of the reported performance of conventional and metamaterial-enhanced Sub-THz MIMO antenna arrays, the major antenna and MIMO performance metrics identified in the reviewed studies are synthesized in Table III. The comparison includes port isolation, radiation efficiency, Envelope Correlation Coefficient (ECC), Diversity Gain (DG), and Channel Capacity Loss (CCL). These metrics collectively provide an assessment of the effectiveness of metamaterial-based decoupling structures in reducing mutual coupling while maintaining or improving the overall MIMO performance.

Table III. Comparative Synthesis of MIMO Performance Metrics for Baseline and Metamaterial-Enhanced Sub-THz Patch Arrays

Performance Metric	Baseline Sub-THz Patch Array (Without MTM)	Metamaterial-Enhanced Array (With MTM)	Reported/Expected System-Level Benefit
Port Isolation (S_{21})	−10 to −14 dB	−25 to −38 dB	Reduced inter-port electromagnetic coupling and associated unwanted power transfer
Radiation Efficiency	50–65%	80–92%	Higher fraction of accepted RF power converted into radiated power
Envelope Correlation Coefficient (ECC)	0.15–0.40	< 0.001	Lower correlation between antenna elements and improved spatial diversity
Diversity Gain (DG)	7.5–8.8 dB	> 9.95 dB	Improved diversity performance and potentially enhanced link reliability
Channel Capacity Loss (CCL)	0.6–1.2 bits/s/Hz	< 0.2 bits/s/Hz	Lower degradation of MIMO channel capacity

As summarized in Table III, the reviewed studies generally report improved port isolation and radiation efficiency for metamaterial-enhanced configurations compared with conventional antenna arrays. The reported lower ECC and CCL values further indicate reduced correlation and lower channel-capacity degradation, while the reported DG values suggest improved diversity performance. However, these values represent results reported across different antenna configurations and operating conditions; therefore, direct comparison should be made with consideration of the differences in frequency, substrate, antenna geometry, element spacing, and evaluation methodology. The observed improvements indicate the potential of metamaterial-based decoupling approaches for compact and high-performance Sub-THz MIMO antenna systems.

5. ADVANCED FABRICATION AND ANTENNA-IN-PACKAGE (AiP) INTEGRATION

Transitioning metamaterial-based microstrip patch antennas to the Sub-THz regime (100–300 GHz) introduces stringent fabrication tolerances, increased material and conductor losses, and significant thermal and packaging challenges. At these frequencies, even small variations in feature dimensions, substrate properties, surface roughness, and alignment can influence the electromagnetic response of the antenna and metamaterial structures.

5.1 Fabrication Technologies at Sub-THz Frequencies At sub-millimeter wavelengths, conventional Printed Circuit Board (PCB)-based fabrication approaches can become increasingly challenging because reduced feature dimensions, etching tolerances, surface roughness, and alignment errors can significantly influence antenna and metamaterial performance [44-46].

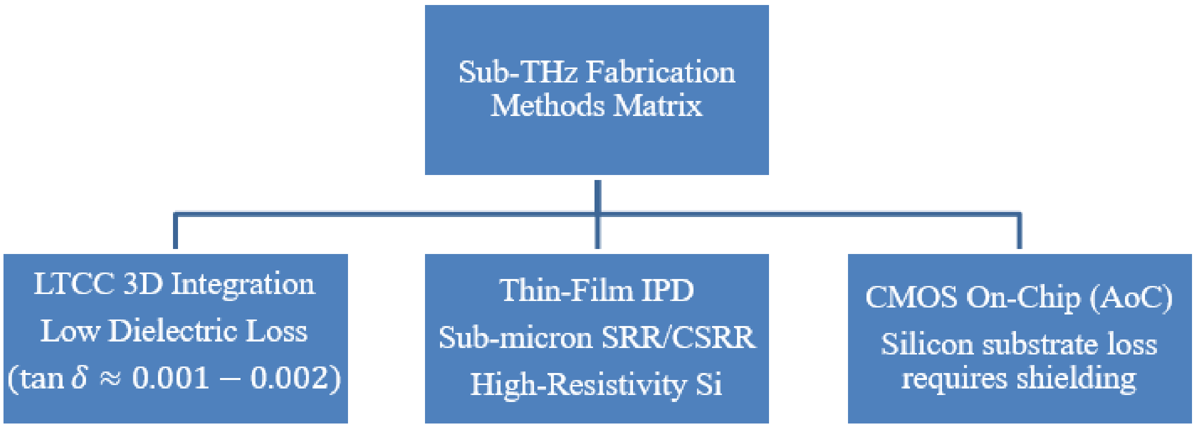

FIGURE 5. Classification matrix of Sub-THz microstrip patch and metamaterial fabrication methods detailing key material and loss characteristics.

Sub-THz metamaterial and antenna structures therefore require fabrication approaches capable of achieving the required dimensional accuracy and material-property control. Three representative technology platforms discussed in this review are Low-Temperature Co-Fired Ceramic (LTCC), Thin-Film Integrated Passive Devices (IPD), and CMOS-based On-Chip Antennas (AoC) [47].

- **Low-Temperature Co-Fired Ceramic (LTCC):** Enables multilayer three-dimensional integration of microstrip patches and embedded EBG structures and can provide relatively low dielectric losses. Its multilayer integration capability makes LTCC attractive for compact Sub-THz antenna and packaging applications [47].
- **Integrated Passive Devices (IPD) / Thin-Film Technology:** Enables fine-pattern fabrication of passive and metamaterial structures, including SRR/CSRR-type geometries, on substrates such as high-resistivity silicon (HR-Si) or quartz. These technologies are suitable for highly integrated Sub-THz antenna implementations [48].
- **CMOS On-Chip Antennas (AoC):** Integrate radiating antenna structures with silicon-based circuits, providing a highly compact implementation for Sub-THz systems. However, substrate-related conductive and dielectric losses can reduce radiation efficiency, motivating the use of appropriate substrate engineering and electromagnetic enhancement techniques [49, 50].

In addition to fabrication and integration constraints, several emerging research directions are relevant to the development of practical and energy-efficient Sub-THz metamaterial-based antenna systems. These include reconfigurable metasurfaces for adaptive electromagnetic control, AI-assisted optimization for efficient metamaterial design, and standardized benchmarking approaches for evaluating energy-related performance. The major challenges and potential research directions are summarized in Table IV.

Table IV. Emerging research challenges and potential directions for metamaterial-based Sub-THz antenna systems.

Research Area	Current Challenge	Potential Metamaterial Research Direction
Reconfigurable Metasurfaces	Fixed-frequency responses may limit adaptability to dynamic beamforming and changing channel conditions.	Integration of tunable materials such as graphene or liquid crystals, along with appropriate biasing and control mechanisms, to enable dynamically reconfigurable electromagnetic responses.
AI-Driven Optimization	Electromagnetic optimization of complex metamaterial unit cells can require substantial computational resources and simulation time.	Utilization of Deep Reinforcement Learning (DRL), surrogate models, and generative approaches to accelerate automated sub-wavelength unit-cell and antenna optimization.
Green Metric Benchmarking	Energy-related performance indicators are not consistently defined or reported across the literature.	Development of standardized evaluation criteria for comparing RF losses, radiation efficiency, decoupling performance, and metamaterial footprint.

6. CONCLUSION

This systematic literature review comprehensively evaluated metamaterial-based mutual coupling reduction techniques for Sub-THz (100 GHz to 300 GHz) microstrip patch MIMO antenna arrays, focusing on achieving high spatial diversity and energy-efficient Green Communication. Operating in the sub-millimeter wave spectrum forces array elements into sub-wavelength spatial proximity, which triggers severe near-field electromagnetic interactions and surface wave propagation. These unwanted coupling effects severely degrade radiation efficiency, distort beamforming patterns, and cause substantial RF power waste in Sub-THz power amplifiers. By analyzing key literature screened through a four-stage PRISMA 2020 process, this review structured state-of-the-art decoupling methods into four main architectural classes: Electromagnetic Bandgap (EBG) surfaces, Split-Ring Resonators (SRR/CSRR), Defected Ground Structures (DGS), and Dynamic Metasurfaces.

Quantitative synthesis of the literature confirms that integrating metamaterial decoupling mechanisms yields transformative performance enhancements across key wireless metrics. Metamaterial structures successfully boost port isolation (ΔS_{21})from typical unisolated levels to over 35 dB, effectively neutralizing inter-element interference at element spacings well below half a wavelength $d < \lambda_0/2$.This isolation improvement suppresses the Envelope Correlation Coefficient (ECC) below 0.001, allowing the Diversity Gain (DG) to reach near-theoretical limits (>9.95 dB) and reducing Channel Capacity Loss (CCL) below 0.2 bits/s/Hz. Furthermore, suppressing parasitic near-field leakage restores radiation efficiency to 85-90%, mitigating thermal power dissipation and directly supporting the energy-efficiency requirements of sustainable 6G terminals.

Despite these electromagnetic benefits, transitioning metamaterial-decoupled arrays from theoretical design to practical deployment introduces significant physical implementation challenges. As detailed in the review of Sub-THz fabrication, dimensional tolerances as small as $2 - 5\ \mu m$ can cause substantial resonant frequency shifts, while sub-micron copper surface roughness significantly increases RF attenuation. Addressing these bottlenecks requires advancing high-precision integration platforms such as Low-Temperature Co-Fired Ceramics (LTCC), Thin-Film Integrated Passive Devices (IPD), and CMOS On-Chip Antennas (AoC). Future research must focus on bridging the gap between electromagnetic metasurface synthesis and scalable nano-fabrication, leveraging automated deep reinforcement learning for unit-cell optimization and dynamic graphene-based metasurfaces to enable adaptive, sustainable 6G wireless infrastructure.

7. FUTURE SCOPE AND RESEARCH DIRECTIONS

While metamaterial-based microstrip patch MIMO arrays demonstrate significant potential for 6G Sub-THz communications, several critical research avenues must be addressed to transition these theoretical and simulated structures into scalable, deployment-ready commercial systems.

AI-Driven Automated Metasurface Synthesis: Conventional electromagnetic (EM) design of sub-wavelength unit cells relies heavily on manual parameter sweeps and computationally expensive full-wave simulations. Future research must leverage Deep Reinforcement Learning (DRL), Physics-Informed Neural Networks (PINNs), and generative AI models to automate unit-cell synthesis. Machine-learning pipelines can rapidly optimize non-intuitive, arbitrary geometric shapes for ultra-wideband surface wave suppression, drastically cutting design cycles and maximizing decoupling efficiency per footprint area.

Dynamic and Adaptive Metasurfaces: Most existing Sub-THz decoupling structures utilize static geometries with fixed operating bandwidths. As 6G networks shift toward dynamic beam-steering and dynamic spatial multiplexing, static bandgap structures become insufficient. Future developments should prioritize integrating active tunable materials—such as Graphene, Liquid Crystals (LCs), and Phase-Change Materials (PCMs like VO_2 to realize reconfigurable metasurfaces. Voltage-tunable surface plasmon polariton (SPP) excitation will enable real-time, dynamic isolation control tailored to real-time beamforming angles.

Advanced Heterogeneous Packaging and Thermal Co-Design: Integrating metamaterial arrays into compact Antenna-in-Package (AiP) and Antenna-on-Chip (AoC) modules requires overcoming strict thermal and physical limitations. Future work must focus on multi-physics co-design strategies that balance electromagnetic isolation, mechanical rigidity, and thermal dissipation. Research into high-conductivity low-loss substrates (e.g., Synthetic Diamond, Quartz, and High-Resistivity Silicon) combined with additive 3D nano-printing will be essential to mitigate surface-roughness losses and structural deformation under high thermal loads.

Standardized Green Metric Benchmarking: Despite the clear theoretical link between mutual coupling reduction and terminal power savings, the literature currently lacks standardized benchmarks for energy efficiency in decoupling topologies. Future research must establish unified IEEE/ITU metrics that explicitly evaluate power amplifier power-added efficiency (PAE) restoration, thermal load mitigation, and active reflection loss reduction relative to the metamaterial footprint. Standardized testing frameworks will provide researchers with a clear roadmap to optimize antennas for true energy sustainability in 6G green communication networks.

References:

1. S. Senger and P. K. Malik, "A comprehensive survey of massive-MIMO based on 5G antennas," *Int. J. RF Microw. Comput.-Aided Eng.*, vol. 32, no. 12, Art. no. e23496, Dec. 2022.

2. Z. Zhang, "Massive MIMO technology: A key advancement in shaping communication networks for the 5G/5G+ era," in *Proc. Int. Wireless Commun. Mobile Comput. (IWCMC)*, May 2024, pp. 274–278.
3. R. Dilli, "Analysis of 5G wireless systems in FR1 and FR2 frequency bands," in *Proc. 2nd Int. Conf. Innov. Mech. Ind. Appl. (ICIMIA)*, Mar. 2020, pp. 767–772.
4. ITU-R, "Requirements, evaluation criteria and submission templates for the development of IMT-2020," Report ITU-R M.2411-0, 2017.
5. M. S. Sharawi, "Current systems and future trends in multi-antenna systems for handsets," *IEEE Antennas Propag. Mag.*, vol. 60, no. 3, pp. 62–70, June 2018.
6. T. Bird, *Mutual Coupling Between Antennas*. Hoboken, NJ, USA: Wiley, 2021.
7. Y. Wang, L. Sun, Z. Du, and Z. Zhang, "Antenna design for modern mobile phones: A review," *Electromagn. Sci.*, vol. 2, no. 2, pp. 1–36, June 2024.
8. M. J. Page et al., "The PRISMA 2020 statement: An updated guideline for reporting systematic reviews," *BMJ*, vol. 372, Art. no. n71, Mar. 2021.
9. N. Donthu, S. Kumar, D. Mukherjee, N. Pandey, and W. M. Lim, "How to conduct a bibliometric analysis: An overview and guidelines," *J. Bus. Res.*, vol. 133, pp. 285–296, Sept. 2021.
10. P. Kaur, S. Malhotra, and M. Sharma, "A review of isolation techniques for 5G MIMO antennas," *J. Telecommun. Inf. Technol.*, no. 3, pp. 43–50, Sept. 2024.
11. D. Gangwar, S. Das, and R. L. Yadava, "Reduction of mutual coupling in metamaterial based microstrip antennas: The progress in last decade," *Wireless Pers. Commun.*, vol. 77, no. 4, pp. 2747–2770, Aug. 2014.
12. J. A. Tirado-Mendez et al., "Metamaterial split-ring resonators applied as reduced-size four-port antenna array for MIMO applications," *AEU-Int. J. Electron. Commun.*, vol. 154, Art. no. 154338, Sept. 2022.
13. P. B. Nikam, J. Kumar, V. Sivanagaraju, and A. Baidya, "Dualband reconfigurable EBG loaded circular patch MIMO antenna using defected ground structure (DGS) and PIN diode integrated branchlines (BLs)," *Measurement*, vol. 195, Art. no. 111127, May 2022.
14. U. Banerjee, S. Sundar Pattanayak, A. K. Biswas, and S. Sahoo, "Design and analysis of a high-isolation metamaterial-inspired MIMO antenna with defected patch structures for improved sub-6 GHz band performance in 5G wireless applications," *Results Eng.*, vol. 28, Art. no. 108280, Dec. 2025.
15. T. Shabbir et al., "16-port non-planar MIMO antenna system with near-zero-index (NZI) metamaterial decoupling structure for 5G applications," *IEEE Access*, vol. 8, pp. 157946–157958, 2020.
16. L. Si, H. Jiang, X. Lv, and J. Ding, "Broadband extremely close-spaced 5G MIMO antenna with mutual coupling reduction using metamaterial-inspired superstrate," *Opt. Express*, vol. 27, no. 3, pp. 3472–3482, Feb. 2019.
17. J. Zaid and A. Z. Ashoor, "Mutual coupling reduction using octagon frequency selective surface structure for full duplex applications," in *Proc. Int. Conf. Electromagnetics Adv. Appl. (ICEAA)*, Oct. 2023, pp. 64–68.
18. Z. Yang, J. Xiao, and Q. Ye, "Enhancing MIMO antenna isolation characteristic by manipulating the propagation of surface wave," *IEEE Access*, vol. 8, pp. 115572–115581, 2020.

19. S. K. Koul, G. S. Karthikeya, A. K. Poddar, and U. L. Rohde, "Using metamaterials in mmWave 5G antennas," *Microw. J.*, vol. 67, no. 6, pp. 40–42, 2024.
20. B. R. Perli et al., "Design and theory of characteristic mode analysis (TCMA) of 4 × 4 high isolation MIMO antenna for sub-6 GHz 5G communications," *Results Opt.*, vol. 21, Art. no. 100903, Dec. 2025.
21. L. Malviya, R. K. Panigrahi, and M. V. Kartikeyan, *MIMO Antennas for Wireless Communication*. Boca Raton, FL, USA: CRC Press, 2020.
22. M. Seyyedesfahlan, A. Uzun, A. K. K. Skrivervik, and I. Tekin, "Wideband multiport antennas," *Sensors*, vol. 20, no. 23, Art. no. 6960, Dec. 2020.
23. A. Aalili and M. Boulouird, "Spectral and energy efficiency in cell-free massive MIMO systems for 5G and 6G wireless communications," in *Proc. 3rd Int. Conf. Electr., Comput., Commun. Mechatronics Eng. (ICECCME)*, July 2023, pp. 1–6.
24. G. Singh et al., "Frequency reconfigurable quad-element MIMO antenna with improved isolation for 5G systems," *Electronics*, vol. 12, no. 4, Art. no. 796, Feb. 2023.
25. T. Durukan and Y. Altuncu, "A compact 4×4 reconfigurable MIMO antenna design with adjustable suppression of certain frequency bands within the UWB frequency range," *AEU-Int. J. Electron. Commun.*, vol. 170, Art. no. 154848, Oct. 2023.
26. S. Akkader, H. Bouyghf, and A. Baghdad, "Miniaturization trends in substrate integrated waveguide for microwave communication systems," in *Proc. 2nd Int. Conf. Innov. Res. Appl. Sci., Eng. Technol. (IRASET)*, Mar. 2022, pp. 1–4.
27. T. Saeidi et al., "High gain triple-band metamaterial-based antipodal Vivaldi MIMO antenna for 5G communications," *Micromachines*, vol. 12, no. 3, Art. no. 250, Feb. 2021.
28. ICNIRP, "Guidelines for limiting exposure to electromagnetic fields (100 kHz to 300 GHz)," *Health Phys.*, vol. 118, no. 5, pp. 483–524, May 2020.
29. A. Ahmed, U. Keshwala, V. Kumari, and S. K. Dubey, "Specific absorption rate analysis for mitigation of electromagnetic hazards in laboratory environment using a miniaturized antenna at 2.45 GHz," *Measurement*, vol. 250, Art. no. 117135, June 2025.
30. M. I. Hossain, M. R. I. Faruque, and M. T. Islam, "Investigation of hand impact on PIFA performances and SAR in human head," *J. Appl. Res. Technol.*, vol. 13, no. 4, pp. 447–453, Aug. 2015.
31. V. Farré, J. Vega-Sánchez, V. Garzón, N. O. Garzón, H. C. Mora, and E. E. Benitez Olivo, "Design and performance analysis of Sub-THz/THz mini-cluster architectures for dense urban 5G/6G networks," *Sensors*, vol. 25, no. 21, Art. no. 6717, Nov. 2025, doi: 10.3390/s25216717.
32. W. Shang, Y. Liao, V. Friderikos, and H. Yanikomeroglu, "Unlocking Sub-THz by robotic aerial base stations: Joint deployment and wireless backhaul routing," *IEEE Open J. Commun. Soc.*, vol. 5, pp. 4880–4896, 2024, doi: 10.1109/OJCOMS.2024.3444857.
33. S. Shome, S. Das, S. Das, and D. Pal, "An extensive review of THz communication in 6G: Facilitating technologies with edge computing and native AI," *Franklin Open*, vol. 13, Art. no. 100434, Dec. 2025, doi: 10.1016/j.fraope.2025.100434.
34. I. F. Akyildiz, J. M. Jornet, and C. Han, "Terahertz band: Next frontier for wireless communications," *Phys. Commun.*, vol. 12, pp. 16–32, Sept. 2014, doi: 10.1016/j.phycom.2014.01.006.

35. K. B. Letaief, W. Chen, Y. Shi, J. Zhang, and Y.-J. A. Zhang, "The roadmap to 6G: AI empowered wireless networks," *IEEE Commun. Mag.*, vol. 57, no. 8, pp. 84–90, Aug. 2019, doi: 10.1109/MCOM.2019.1900271.
36. X. Li, Z. Li, M. Chen, M. Bennis, and M. Debbah, "Green AI for 6G networks: Resource optimization and sustainability," *IEEE Commun. Mag.*, vol. 61, no. 1, pp. 102–108, Jan. 2023, doi: 10.1109/MCOM.001.2200103.
37. W. Jiang, Q. Zhang, J. He, M. A. Habibi, S. Melnyk, M. El-Absi, B. Han, M. Di Renzo, H. D. Schotten, F.-L. Luo, T. S. El-Bawab, M. Juntti, M. Debbah, and V. C. M. Leung, "Terahertz communications and sensing for 6G and beyond: A comprehensive review," *IEEE Commun. Surv. Tutor.*, vol. 26, no. 4, pp. 2326–2381, 4th Quart. 2024, doi: 10.1109/COMST.2024.3385908.
38. W. M. Othman, A. A. Ateya, M. E. Nasr, A. Muthanna, M. ElAffendi, A. Koucheryavy, and A. A. Hamdi, "Key enabling technologies for 6G: The role of UAVs, terahertz communication, and intelligent reconfigurable surfaces in shaping the future of wireless networks," *J. Sens. Actuator Netw.*, vol. 14, no. 2, Art. no. 30, Mar. 2025, doi: 10.3390/jsan14020030.
39. A. Faisal, H. Sarieddeen, H. Dahrouj, T. Y. Al-Naffouri, and M.-S. Alouini, "Ultra-massive MIMO systems at terahertz bands: Prospects and challenges," *IEEE Veh. Technol. Mag.*, vol. 15, no. 4, pp. 33–42, Dec. 2020, doi: 10.1109/MVT.2020.3022998.
40. Z. Chen, B. Ning, C. Han, Z. Tian, and S. Li, "Intelligent reflecting surface assisted terahertz communications toward 6G," *IEEE Wirel. Commun.*, vol. 28, no. 6, pp. 110–117, Dec. 2021, doi: 10.1109/MWC.001.2100215.
41. C. Jiang, H. Zhang, Y. Ren, Z. Han, K. Chen, and L. Hanzo, "Machine learning paradigms for next-generation wireless networks," *IEEE Wirel. Commun.*, vol. 24, no. 2, pp. 98–105, Apr. 2017, doi: 10.1109/MWC.2017.1600300WC.
42. M. Sode, M. Ponschab, L. N. Ribeiro, S. Haesloop, E. Tohidi, M. Peter, W. Keusgen, A. Schultze, P. Sroka, and B. Schroeder, "Reconfigurable intelligent surfaces for 6G mobile networks: An industry R&D perspective," *IEEE Access*, vol. 12, pp. 159820–159840, 2024, doi: 10.1109/ACCESS.2024.3485227.
43. Z. Zhang, Y. Xiao, Z. Ma, M. Xiao, Z. Ding, X. Lei, G. K. Karagiannidis, and P. Fan, "6G wireless networks: Vision, requirements, architecture, and key technologies," *IEEE Veh. Technol. Mag.*, vol. 14, no. 3, pp. 28–41, Sept. 2019, doi: 10.1109/MVT.2019.2928686.
44. R. Chataut, M. Nankya, and R. Akl, "6G networks and the AI revolution—Exploring technologies, applications, and emerging challenges," *Sensors*, vol. 24, no. 6, Art. no. 1888, Mar. 2024, doi: 10.3390/s24061888.
45. D. C. Larsson, A. Grövlen, S. Parkvall, and O. Liberg, "6G standardization – An overview of timeline and high-level technology principles," *Ericsson Blog*, Mar. 22, 2024. [Online]. Available: https://www.ericsson.com/en/blog/2024/3/6g-standardization-timeline-and-technology-principles
46. H.-J. Song and N. Lee, "Terahertz communications: Challenges in the next decade," *IEEE Trans. Terahertz Sci. Technol.*, vol. 12, no. 2, pp. 105–117, Mar. 2022, doi: 10.1109/TTHZ.2021.3129520.
47. S. H. Kim, T. H. Jang, D. M. Kang, K. P. Jung, and C. S. Park, "Wideband 120-GHz CMOS I/Q transmitter with suppressed IMRR and LOFT for wireless short-range high-speed 6G IoT applications," *IEEE Internet Things J.*, vol. 10, no. 13, pp. 11739–11748, July 2023, doi: 10.1109/JIOT.2023.3243178.

48. T. S. Rappaport, Y. Xing, O. Kanhere, S. Ju, A. Madanayake, S. Mandal, A. Alkhateeb, and G. C. Trichopoulos, "Wireless communications and applications above 100 GHz: Opportunities and challenges for 6G and beyond," *IEEE Access*, vol. 7, pp. 78729–78757, 2019, doi: 10.1109/ACCESS.2019.2921522.
49. A. Armghan, V. Mandaliya, M. Alsharari, K. Aliqab, S. Ben Chaabane, and A. Flah, "Development and enhancement of metamaterial-inspired Ag-GaAs THz MIMO antenna with optimized diversity metrics using data-driven machine learning algorithms for future 6G networks," *Sci. Rep.*, vol. 15, Art. no. 43901, Dec. 2025, doi: 10.1038/s41598-025-83901-w.
50. G. C. Alexandropoulos, N. Shlezinger, I. Alamzadeh, M. F. Imani, H. Zhang, and Y. C. Eldar, "Hybrid reconfigurable intelligent metasurfaces: Enabling simultaneous tunable reflections and sensing for 6G wireless communications," *IEEE Veh. Technol. Mag.*, vol. 19, no. 1, pp. 75–84, Mar. 2024, doi: 10.1109/MVT.2023.3332580.